Chinese Journal of Aeronautics, (2016), 29(1): 129–143

Chinese Society of Aeronautics and Astronautics
& Beihang University

Chinese Journal of Aeronautics

cja@buaa.edu.cn
www.sciencedirect.com

Characteristic analysis of lock-in for an elastically suspended airfoil in transonic buffet flow

Quan Jingge *, **Zhang Weiwei, Gao Chuanqiang, Ye Zhengyin**

School of Aeronautics, Northwestern Ploytechnical University, Xi'an 710072, China

Received 21 January 2015; revised 29 June 2015; accepted 3 August 2015
Available online 21 December 2015

KEYWORDS

Aeroelastic analysis;
Buffet;
Elastic airfoil;
Lock-in;
Transonic flow

Abstract Numerical simulations are performed to study the aeroelastic responses of an elastically suspended airfoil in transonic buffet flow, by coupling the unsteady Reynolds-averaged Navier-Stokes (RANS) equations and structural motion equation. The current work focuses on the characteristic analysis of the lock-in phenomenon. Great attentions are paid to studying the frequency range of lock-in and the effects of the three parameters, namely the structural natural frequency, mass ratio and structural damping, on lock-in characteristic of the elastic system in detail. It is found that when the structural natural frequency is close to the buffet frequency, the coupling frequency of the elastic system is no longer equal to the buffet frequency, but keeps the same value as the structural natural frequency. The frequency lock-in occurs and stays present until the structural nature frequency is near the double buffet frequency. It means that the lock-in presents within a broad range, of which the lower threshold is near the buffet frequency, while the upper threshold is near the double buffet frequency. Moreover, the frequency range of lock-in is affected by mass ratio and structural damping. The lower the mass ratio and structural damping are, the wider the range of lock-in will be. The upper threshold of lock-in grows with the mass ratio and structural damping decreasing, but the lower threshold always keeps the same.

1. Introduction

In transonic flow, due to the shock-boundary-layer interaction, the self-sustained, low frequency, large amplitude shock oscillations along the airfoil chord are observed for certain combinations of Mach number and mean angle of attack, even in the absence of airfoil motion. We define it as shock buffet. The transonic buffet flow is so highly unsteady and nonlinear, making the corresponding study on flow stability difficult and complicated. So far, there is not yet a clear mechanism which can fully explain the transonic shock buffet phenomenon. Lee[1] proposed a self-sustained feedback model to explain the mechanism of shock oscillation, but there were some defects. Crouch et al.[2,3] provided a new perspective to study the mechanism of transonic buffet from the view of global instability, but still had its flaw. The actual transonic shock buffet

* Corresponding author. Tel.: +86 29 88491342.
E-mail address: pigeon729@163.com (J. Quan).
Peer review under responsibility of Editorial Committee of CJA.

Production and hosting by Elsevier

http://dx.doi.org/10.1016/j.cja.2015.12.002
1000-9361

mechanism is still a subject of discussion and worthy of a long deep fine study.

For a long time, a large number of experiments[4,5] and numerical simulation researches[6–11] are carried out on transonic shock buffet phenomena, but mostly focus on the rigid airfoil and always study the prediction of the buffet onset. There are less studies on the transonic buffet characteristics of the elastic airfoil, even less on the buffet responses. In the classic concept of aeroelasticity, buffet is usually defined as forced vibration. Under this condition, the aerodynamic loads have no relation with structure motion, so it is not necessary to analyze buffet by coupling the aerodynamic loads with structure motion. The influences of the structural elastic mode on flow characteristics and aeroelastic responses can be ignored. However, the practical aerodynamic load is not only related to flow state (Mach number, angle of attack, dynamic pressure, et al.), but also associated with structure vibration more or less. The airfoil structural motion can affect flow characteristics to a certain extent and present obvious fluid-structure interaction characteristic. Steimle et al.[12] carried out unsteady transonic flow experiments on elastic wing. It is clearly shown that the interaction of shock/boundary-layer and separated flow produces huge pressure fluctuations and also results in a strong fluid-structure coupling. Therefore, the elastic effect of the airfoil and the associated buffet response problem should not be ignored in transonic buffet analysis.

In recent years, numerical simulations have been carried out to investigate the effects of prescribed airfoil harmonic oscillation on flow patterns and responses characteristics via uncoupled method and the lock-in phenomenon has been observed. Raveh and Dowell[13,14] simulated the response of a prescribed oscillation airfoil in transonic buffet flow and found that lock-in occurred when the shock buffet frequency synchronized with the prescribed airfoil pitch motion frequency and the amplitude was above a certain threshold. The system response predominantly assumed the frequency of the airfoil motion. Iovnovich and Raveh[15] found that resonance and phase lead appeared near the buffet onset when the airfoil forced movement frequency was close to the buffet frequency. Nitzsche and Giepman[16] studied the aerodynamic resonance response of a two-dimensional (2-D) airfoil under pre-buffet flow conditions to prescribed harmonic flap, pitch, and translational motions. Young and Lai[17] found the vortex lock-in phenomenon in the case of an oscillating airfoil in plunge at Reynolds number of 2.0×10^4. Harmann et al.[18] carried out experiments to study the influence of coupled heave and pitch oscillations in the transonic flow. It was found that at forced oscillation at excitation frequencies in the buffet range, the shock oscillation locked into the excitation frequency indeed. Although the above-mentioned studies considered the influence of structure vibration on flow characteristic and found the lock-in phenomenon, they did not analyze the effect of the elastic mode on the buffet flow and response characteristics.

When considering the elastic effect of the structure, the structural movement and the shock buffet oscillation will be interacted with each other, having a significant impact on the transonic buffet flow and aeroelastic responses. Raveh and Dowell[19] firstly studied the aeroelastic response of an elastically suspended airfoil in transonic buffet flow using RANS solver and found the frequency lock-in occurs, when the frequency of the elastic system is close to the buffet frequency and the oscillation amplitude is above some threshold. The study is useful and directive for the lock-in research of an elastic airfoil in transonic buffet flow.

In current study, an aeroelastic system comprised of a NACA0012 airfoil, suspended on a pitch spring, is simulated in transonic buffet flow by coupling the unsteady flow solver with structural motion equation. The work focuses on the characteristic analysis of the lock-in phenomenon, which can be observed in the responses of an elastic airfoil in transonic buffet flow. A series of computations is carried out to mainly study the frequency range of lock-in and the influences of the structural natural frequency, mass ratio and the structural damping on the lock-in characteristics in detail.

2. Numerical method

2.1. Unsteady flow solver

The unsteady transonic buffet flow is simulated by a finite volume method for the unsteady RANS solver. Xiao[7], Iovnovich[8] and Barakos et al.[9] have used the RANS equations to investigate the buffet flow around several 2-D airfoils and have good agreements with experiment datas, which demonstrate that current RANS has good capability to capture shock buffet phenomenon.

Based on Morkovin's assumption, the RANS equations ignore density fluctuations, and approximate turbulence flow as the sum of a mean steady flow and a small-disturbance unsteady flow, which is represented by a turbulent model. The two-dimensional integral governing equations for unsteady Reynolds-averaged Navier-Stokes equations are expressed as[20,21]

$$\frac{\partial}{\partial t}\int\int_{\Omega} \boldsymbol{Q}\mathrm{d}S + \int_{\Gamma} \boldsymbol{F}(\boldsymbol{Q}, \boldsymbol{V}_{\mathrm{grid}}) \cdot \boldsymbol{n}\mathrm{d}\Gamma = \int_{\Gamma} \boldsymbol{G}(\boldsymbol{Q}) \cdot \boldsymbol{n}\mathrm{d}\Gamma \tag{1}$$

where Ω is the control surface element, S the surface, t the time, Γ the boundary of the control surface element, and $\boldsymbol{n}$ the identity normal vector. $\boldsymbol{Q}$, $\boldsymbol{F}(\boldsymbol{Q}, \boldsymbol{V}_{\mathrm{grid}})$, $\boldsymbol{G}(\boldsymbol{Q})$ represent the conservation vector, the inviscid flux vector considering grid moving velocity, and the viscous flux vector respectively. $\boldsymbol{V}_{\mathrm{grid}}$ is the moving grid velocity vector. By dimensional analysis, the equations can be expressed in terms of dimensions of the chord length, free stream density, speed of sound, as well as temperature.

The AUSM + up scheme is adopted for spatial discretization to capture the shock discontinuity accurately and suppress numerical oscillations in space. An implicit dual-time stepping method is used for time discretization to ensure that the numerical method has second-order accuracy in time. At sub-iteration, the fourth stage Runge–Kutta scheme is applied with local-time stepping, also using the residual smoothing technique and multi-grid for convergence acceleration.

The Spalart–Allmaras (S–A) turbulence model is used for all computations. S–A model has good robust and numerical convergence, which can well simulate the attached flow and thin free shear layer flow.

The grid deformation is realized by a radial basis functions (RBF) interpolation scheme.[22] In order to avoid additional

error caused by grid motion, the geometric conservation law is introduced.

2.2. Structural equation of motion

The aeroelastic equation of motion of the one-degree-of-freedom pitch system for the elastically suspended airfoil is

$$I_\alpha\ddot{\alpha} + 2I_\alpha\zeta\omega_\alpha\dot{\alpha} + I_\alpha\omega_\alpha^2\alpha = M \tag{2}$$

where α is the pitch angle of attack, ω_α the pitch natural frequency, and ζ non-dimensional structural damping. The airfoil moment of inertia can be expressed as $I_\alpha = mr_\alpha^2b^2$, in which m is mass, r_α the non-dimensional radius of gyration about elastic axis, and b semi-chord length. The pitch moment term is $M = \frac{1}{2}\rho_\infty v_\infty^2(2b)^2C_m$, assuming the center of pressure as its integrated point. ρ_∞, v_∞, C_m represent the free-stream density, free-stream velocity, and the airfoil moment coefficient respectively.

By defining the non-dimensional time $\tau = \omega_\alpha t$, mass ratio $\mu = \frac{m}{\pi\rho_\infty b^2}$, pitch reduced frequency $k_\alpha = \frac{\omega_\alpha b}{v_\infty}$, and non-dimensional velocity $v^* = \frac{v_\infty}{\omega_\alpha b\sqrt{\mu}} = \frac{1}{k_\alpha\sqrt{\mu}}$, we have the dimensionless aeroelastic motion equation of Eq. (2) as follows:

$$\ddot{\alpha} + 2\zeta\dot{\alpha} + \alpha = \frac{2}{\pi r_\alpha^2}v^{*2}C_m \tag{3}$$

For solving the Eq. (3) simply, the state space method is used to transform Eq. (3) into first-order ordinary differential equations with initial conditions known. By defining a structural state-vector $\boldsymbol{x} = [\xi_1, \xi_2, \cdots, \dot{\xi}_1, \dot{\xi}_2, \cdots]^{\mathrm{T}}$, the structural equation in state-space form is

$$\dot{\boldsymbol{x}} = \boldsymbol{E}(\boldsymbol{x}, t) = \boldsymbol{A}\boldsymbol{x} + \boldsymbol{B}\boldsymbol{Q}'(\boldsymbol{x}, t) \tag{4}$$

where $\boldsymbol{A} = \begin{bmatrix} 0 & 1 \\ -1 & -2\zeta \end{bmatrix}$, $\boldsymbol{B} = \begin{bmatrix} 0 \\ 1 \end{bmatrix}$, $\boldsymbol{Q}'(\boldsymbol{x}, t) = \frac{2}{\pi r_\alpha^2}v^{*2}C_m$.

This paper uses a four-order hybrid linear multi-step scheme[23] to solve Eq. (4), which has been proved of a high efficiency and precision, as well as a good stability.

3. Validation of method

3.1. Test case 1: Vortex-induced vibrations of an elastically mounted cylinder

The lock-in phenomenon is earliest observed in vortex-induced vibrations behind a cylinder. Numerical and wind tunnel investigations[24–27] have been carried out to study the vortex-induced vibrations of a circular cylinder mounted on elastic supports and it is found that the lock-in occurs when the cylinder vibration frequency matches the vortex shedding frequency.

To ascertain the accuracy of current numerical method and its implementation, the vortex-induced vibrations of an elastically mounted cylinder in two dimensions are simulated at low Reynolds number. The cylinder is free to vibrate in both transverse and in-line directions, with a low non-dimensional mass equal to 10. The Reynolds number is fixed (Re = 100) and the reduced natural frequency F_n is varied ($F_n = f_nD/U_\infty$, D is the diameter of the cylinder, U_∞ is the free-stream velocity and f_n is the nature frequency of the cylinder).

The numerical grid is a hybrid unstructured mesh with quadrilateral cells in boundary layer region, as shown in Fig. 1. The computational domain is $60D \times 40D$, with the above twenty thousand points.

As the amplitude of transverse vibrations is much higher than those of in-line oscillations, here we just show the results of the cylinder transverse vibrations. Fig. 2 shows the variation of the transverse displacement of the cylinder with the reduced natural frequency, in which A is the amplitude of the cylinder variation. The cylinder exhibits self-excited oscillations beyond F_n = 0.12. The maximum amplitude is achieved at F_n = 0.20 and the cylinder ceases to vibrate beyond F_n = 0.22. Fig. 3 shows the coupling reduced frequency of the cylinder changes with the reduced natural frequency. When the reduced natural frequency is below 0.12 or above 0.22, the cylinder coupling reduced frequency matches the vortex shedding frequency (the Strouhal number St for the stationary cylinder at Re = 100 is about 0.166). The cylinder exhibits forced vibration induced by the vortex shedding. When the reduced natural frequency is between 0.12 and 0.22, the cylinder coupling reduced frequency synchronizes with the reduced natural frequency. The lock-in is observed.

All the results are in good agreement with those of Singh and Mittal[27], indicating that our computational method is effective and accurate to simulate the lock-in phenomenon.

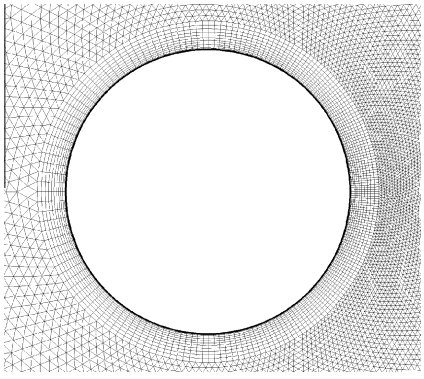

Fig. 1 Numerical grid of cylinder.

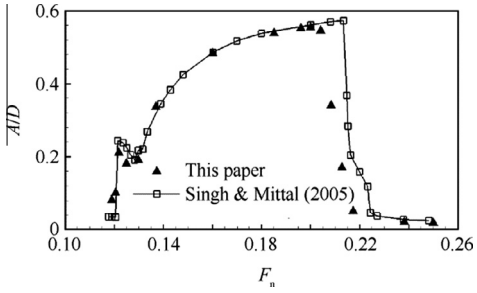

Fig. 2 Transverse displacement of cylinder at various reduced natural frequencies.

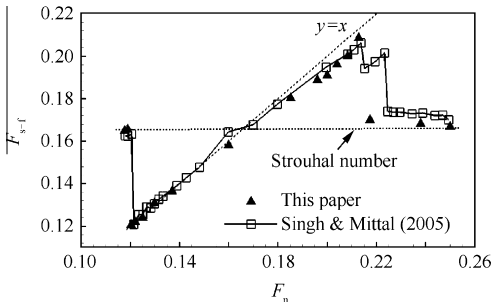

Fig. 3 Coupling reduced frequency of cylinder at various reduced natural frequencies.

3.2. Test case 2: Prediction of shock buffet onset of a rigid airfoil

The transonic buffet flow over a NACA0012 airfoil at Mach number of 0.70 and Reynolds number of 3.0×10^6 is simulated to verify the effectiveness of current numerical method in simulating transonic buffet flow. The computational grid is a 2-D hybrid unstructured mesh with quadrilateral cells in the expected boundary layer region and triangles in outer field. The far field extends 20 chords away from airfoil surface. The computational domain has 200×36 points in boundary layer region and the total nodes are about ten thousand.

Fig. 4 shows the lift and moment coefficient time history at different angles of attack with $Ma = 0.7$, $Re = 3.0 \times 10^6$. For the small mean angle of attack of 4.6°, the amplitudes of the lift and moment coefficient responses tend to be zero, which means that the flow is steady. For the mean angle of attack of 4.7°, the aerodynamic responses begin to oscillate apparently, hinting that the flow is unsteady and shock buffet occurs, although the amplitude is a little small. For the mean angle of attack of 4.8°, the lift and moment responses have dramatic oscillation with a large amplitude of $\Delta C_l = 0.036$, as a result of the present shock buffet. So the shock buffet onset is $\alpha_m = 4.7°$ for the rigid NACA0012 airfoil at $Ma = 0.7$, $Re = 3.0 \times 10^6$. This result agrees well with the wind tunnel experiment datas[28].

Fig. 5 shows the pressure contours at different time instants of a cycle at mean angle of attack of 4.8°. It is seen that the location of shock changes with time. The shock oscillation is clear.

Fig. 6 presents the frequency content of the lift and moment coefficient responses at $Ma = 0.7$, $\alpha_m = 4.8°$. Both of them have a main peak at the same reduced frequency of 0.18, which is the buffet reduced frequency and agrees well with the experiment datas[28]. Besides, the moment coefficient response still consists of another much smaller peak at a high frequency equal to 0.36, which is twice the buffet reduced frequency.

Simulations are repeated for a Mach number range of 0.7–0.78 at various angles of attack including the onset of shock buffet. Fig. 7 shows the prediction results of the shock buffet onset boundary by current numerical method and compares them with the experimental datas.[28] Both of them are in good agreement.

Based on this validation, it is concluded that good prediction of the buffet onset conditions can be achieved via current numerical method.

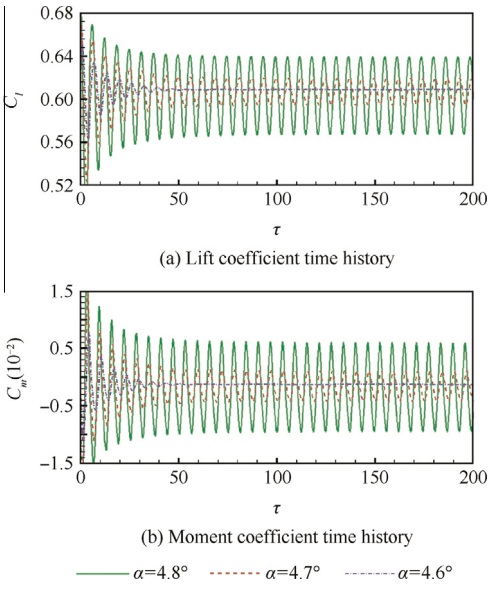

Fig. 4 Lift and moment coefficient time history at different angles of attack with $Ma = 0.7$, $Re = 3.0 \times 10^6$.

4. Aeroelastic analysis of an elastically suspended airfoil

As we know, the shock buffet onset is always a function of Mach number and mean angle of attack. For a rigid airfoil, once buffet occurs at a specific Mach number and angle of attack, the vortex flow characteristic is determined and has a unique natural frequency, which resembles the natural frequency of the structure, usually defined as the shock buffet reduced frequency. When the airfoil is flexible, the unsteady aerodynamic forces, induced by the shock wave oscillation and shock-induced flow separation, exert on the airfoil and result in the airfoil vibration. As the shock buffet frequency is close to the structural natural frequency of the airfoil, resonance may take place within the elastic system. Besides, the airfoil elastic vibration can affect the flow pattern also. They interact with each other, and induce significant aeroelastic responses. Under some conditions, the airfoil elastic vibration may be so large that it may interfere with and control flow pattern, making the elastic system frequency lock into the structural frequency. The lock-in occurs.

The computation case in the current study is that of a NACA0012 airfoil, suspended on a pitch spring in transonic buffet flow. All simulations are performed at Mach number of 0.70 and Reynolds number of 3.0×10^6, with a mean angle of attack of $\alpha = 4.8°$, for which buffet exists with a reduced frequency of $k_f = 0.18$. The numerical grid uses the same grid in Section 3.2. The computational domain is covered by hybrid unstructured grid with quadrilateral cells in boundary layer, extending approximately 20 chords away from the profile.

By current numerical methods, the characteristic of lock-in, which will be present in aeroelastic responses of the elastic airfoil in transonic buffet flow, is studied dominantly. High emphases are put on the frequency range of lock-in, and the effects of the three parameters, which are the structural natural frequency, mass ratio and structural damping, on lock-in characteristics of the elastic system.

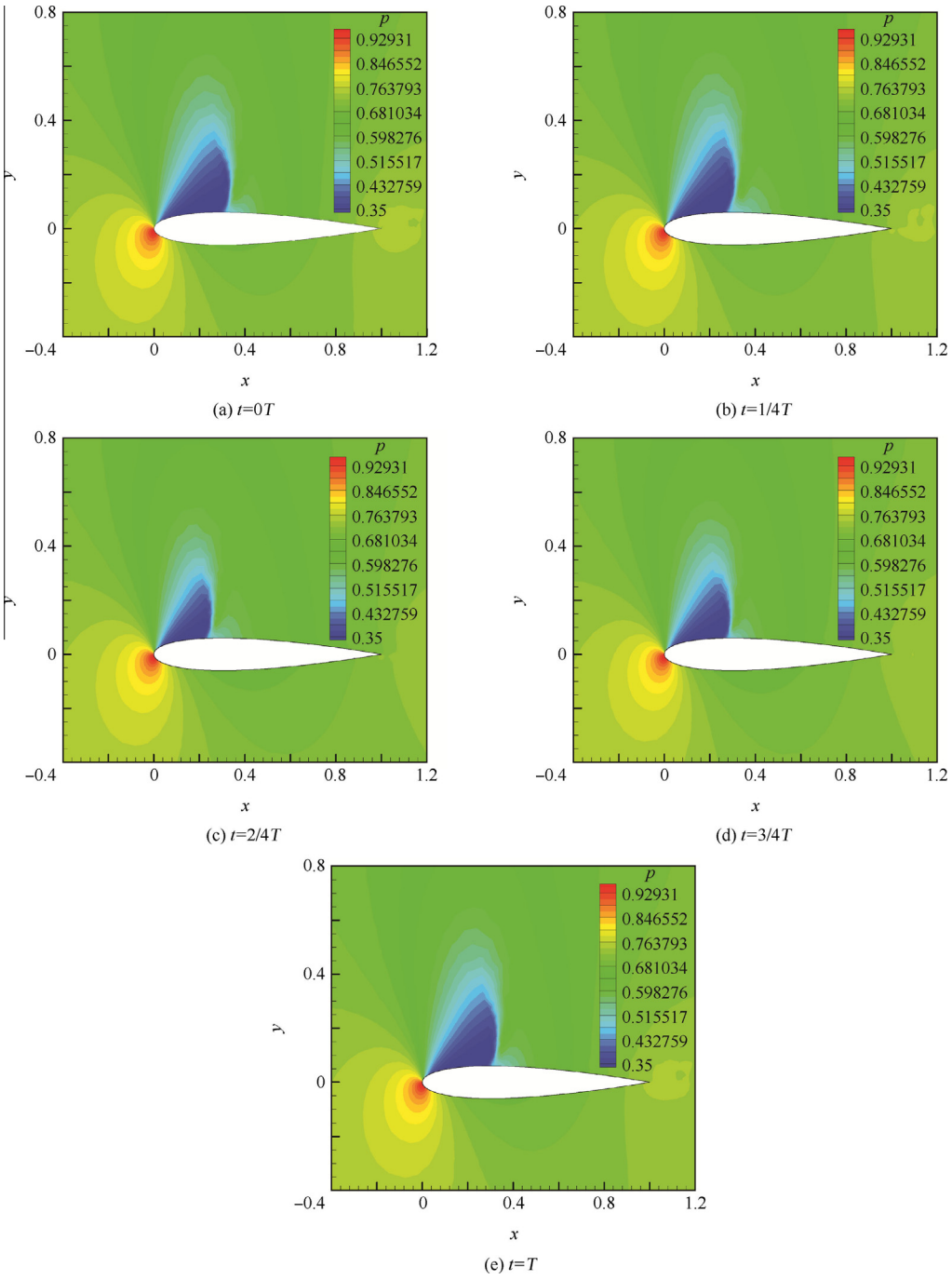

Fig. 5 Pressure contours at different time instants of a cycle at mean angle of attack of 4.8°, $Ma = 0.7$, $Re = 3.0 \times 10^6$.

Before further study, three different and important parameters need to be introduced in advance. They are the structural natural reduced frequency in pitch motion k_α, the shock buffet reduced frequency k_f, and the coupling elastic system reduced frequency k_{s-f} In the later section, they will present many times, so we should keep their differences in mind to avoid confusion. Moreover, all the frequencies present in current paper are non-dimensional reduced frequency.

4.1. Frequency lock-in phenomenon of an elastically suspended airfoil in transonic buffet flow

To investigate the aeroelastic responses of the elastic system in transonic buffet flow, simulations are performed with fixed mass ratio and various natural frequencies, ranging from below to above the shock buffet frequency, as well as neglected structural damping. The simulation conditions are at

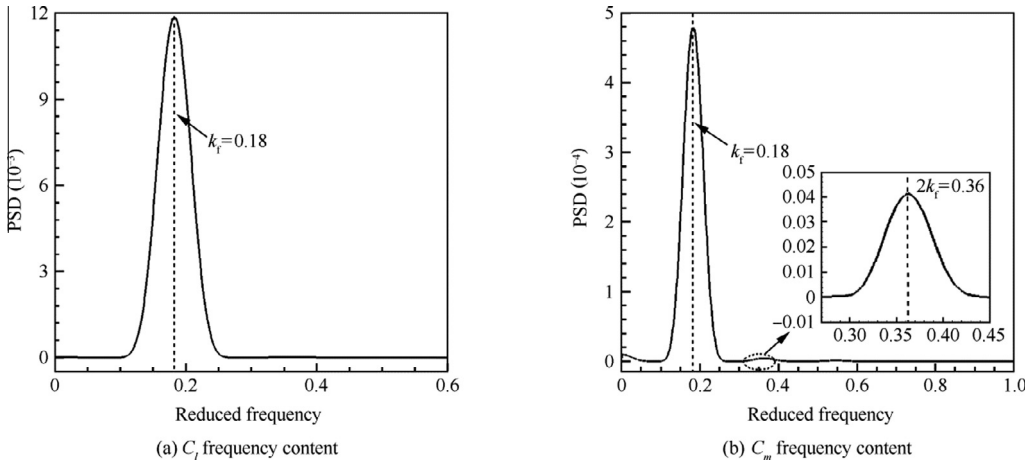

Fig. 6 Frequency content of aerodynamic responses at mean angle of attack of 4.8°, $Ma = 0.7$, $Re = 3.0 \times 10^6$.

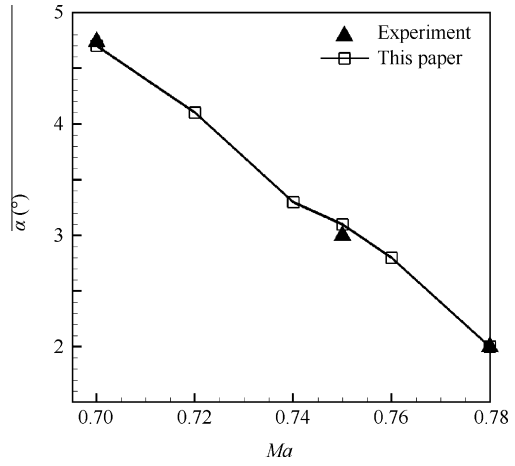

Fig. 7 Transonic buffet onset boundary for a rigid NACA0012 airfoil.

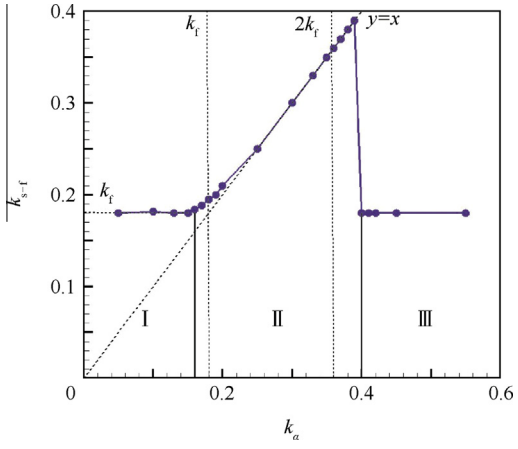

Fig. 8 Coupling frequency of elastic system at different structural natural frequencies with $\mu = 200$, $\zeta = 0$.

$Ma = 0.7$, $\alpha_m = 4.8°$, $Re = 3.0 \times 10^6$, $r_\alpha^2 = 1.036$, $\mu = 200$, $\zeta = 0$, $k_\alpha = 0 - 0.55$.

Fig. 8 shows the coupling frequency of the elastic system at different structural natural frequencies. It is shown that as the structural natural frequency changes, the elastic system exhibits different patterns in different regions.

When the structural natural frequency is far lower than the buffet frequency, the elastic system coupling frequency is equal to the buffet frequency, namely $k_{s-f} = k_f = 0.18$. As shown in region I. The airfoil exhibits forced vibration with small amplitude, so the influence of elastic motion on transonic buffet flow is much weak.

When the structural natural frequency is close to the buffet frequency, the elastic system coupling frequency is no longer equal to, but slowly deviates from the buffet frequency, and shifts towards the structural natural frequency, then finally keeps the same value as the structural natural frequency, namely $k_{s-f} = k_\alpha$. The lock-in occurs. Whereas, when the structural natural frequency is far away from the buffet frequency, the elastic system coupling frequency still locks into the structural natural frequency. The lock-in keeps present until the structural nature frequency is near the double buffet frequency, as shown in region II.

Then, when the structure natural frequency continually increases up to a considerable value, as shown in region III, which is far larger than the double buffet frequency, the system coupling frequency will ultimately leave the structure natural frequency and return back to the buffet frequency, namely $k_{s-f} = k_f$. The lock-in phenomenon vanishes.

The results of Fig. 8 show that as the structural natural frequency changes, the aeroelastic characteristic of the elastic system experiences the lock-in phenomenon. The lock-in presents in a wide range, of which the lower threshold is near the buffet frequency, while the upper threshold is near the double buffet frequency. It is apparent from this figure. In the range of lock-in, the system coupling frequency keeps the same value as the structural natural frequency. Beyond the range of lock-in, the system coupling frequency moves back to the buffet frequency.

Figs. 9–11 present the aeroelastic responses of the elastic system and the corresponding power spectrum density

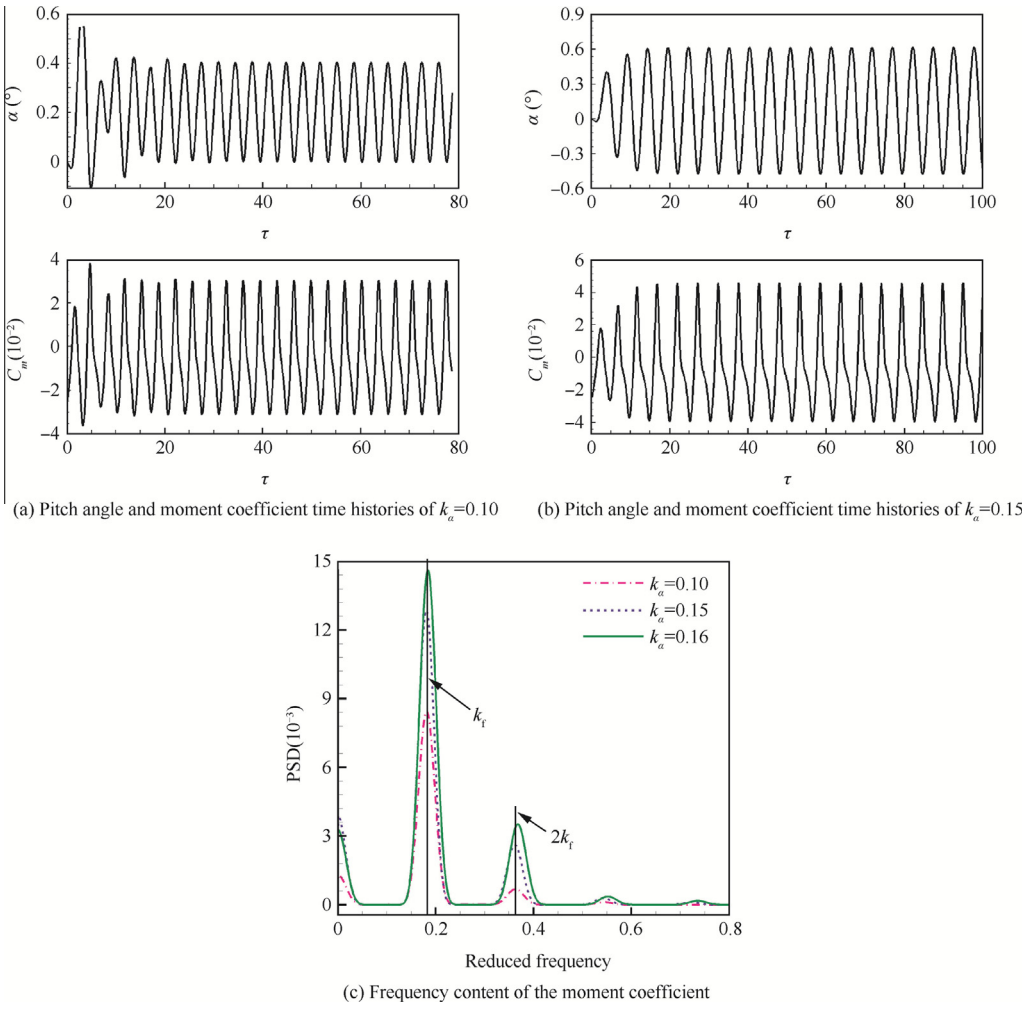

Fig. 9 Aeroelastic responses and frequency content of elastic system at $k_\alpha \ll k_f$.

(PSD) analysis at different structural natural frequencies in detail.

It can be seen from Fig. 9 that when the structure natural frequency is much smaller than the buffet frequency, corresponding to region I in Fig. 8, the pitch angle of attack and moment coefficient curves exhibit a harmonic vibration and the amplitudes rise as the structure natural frequency increases. The system reaches limit cycle oscillation (LCO). The pitch oscillation is just of a very small angle, so it is not enough to affect the transonic buffet flow characteristic. The responses behave forced vibration, and the system coupling frequency is equal to the buffet frequency. Fig. 9(c) shows the corresponding frequency content of moment coefficient. It is seen that the flow has a main peak at the buffet frequency and a secondary smaller peak at the double buffet frequency, as well as other weak higher harmonics.

When the structure natural frequency is in the vicinity of the buffet frequency, as seen in Fig. 10, the pitch angle and moment coefficient curves spread slowly to a weak harmonic vibration, and the system goes into a weak LCO. With the closeness of the structure natural frequency to the buffet frequency, the system reaches resonance and the response amplitude increases. The airfoil elastic motion is large enough to interfere with and control the flow pattern, causing the elastic system frequency to lock into the structural natural frequency. The lock-in occurs. So the frequency content of moment response is shifted from the buffet frequency towards the structure natural frequency and has a double frequency component and other high frequency components, as shown in Fig. 10(c).

When the structural natural frequency is near the double buffet frequency, the pitch angle response is divergent and the divergence speed falls with the structural natural frequency increasing. While the responses of moment coefficient always experience a short period of convergent oscillation at lower frequency firstly, and then diverge slowly with high and low frequencies coexistence, at last totally develop into a high divergent oscillation. As the structural natural frequency increases, the divergence speed and the amplitude fall, but the time of the initial convergent oscillation persists longer. Fig. 11(c) and (d) show the clear time history of moment coefficient at $k_\alpha = 0.33$ and 0.39 respectively. By contrast, the period of convergent oscillation at $k_\alpha = 0.33$ is very short and the system quickly comes into high-frequency divergent oscillation. While, the moment coefficient response at $k_\alpha = 0.39$ beats in cucurbit shape in the first and lasts long before divergence. Frequency analysis of the moment

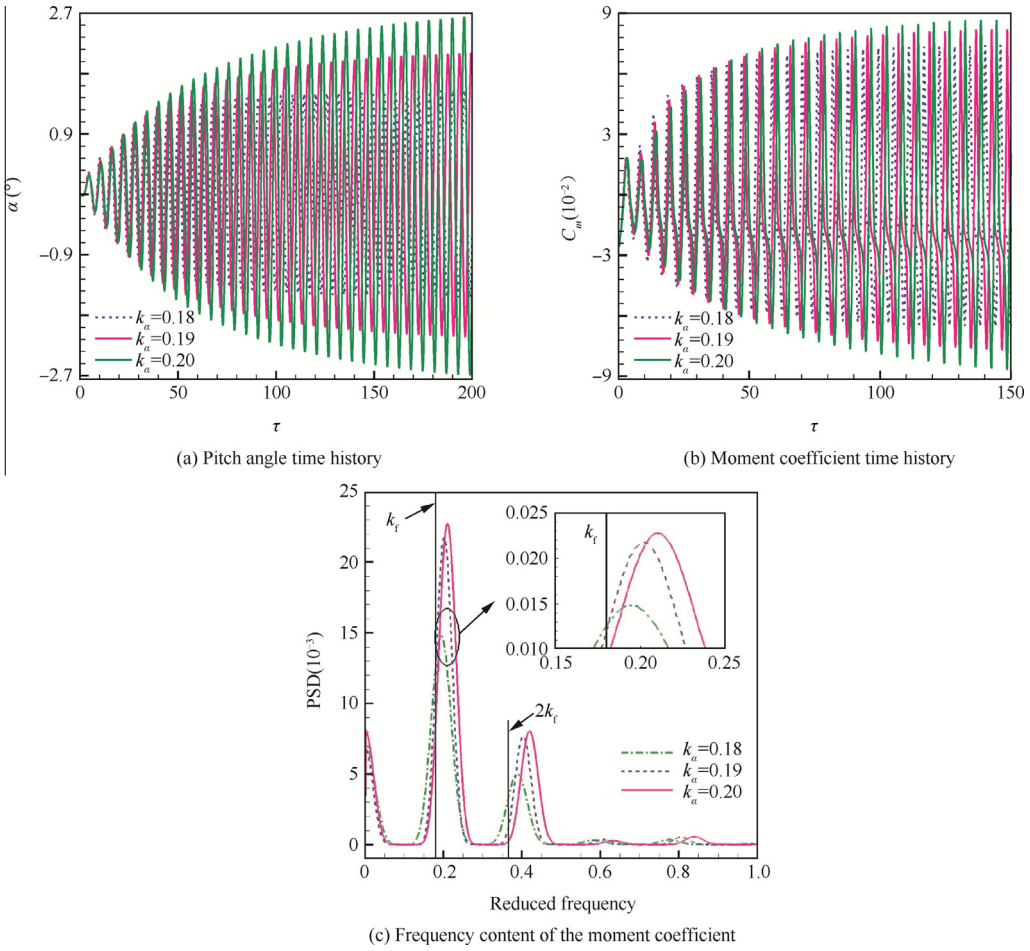

Fig. 10 Aeroelastic responses and frequency content of elastic system when structure frequency is close to buffet frequency.

coefficient response in different time periods is conducted. In the first period of the simulation, the pitch angle is so small that it does not affect flow; therefore the flow is dominated by the shock buffet. The moment response is mainly at the buffet frequency only. In the second period of the simulation, the frequency content of the moment coefficient shows less power in the buffer frequency and more power in the structural natural frequency. It means that as pitch angle grows, the buffet frequency gets weak, while the structural natural frequency becomes strong. Finally, in the last period, the moment frequency content is solely in the structural natural frequency. For this time period, the structural natural frequency dominant in the flow and the buffet frequency vanishes. The lock-in phenomenon occurs.

Fig. 11(e) presents the frequency content of moment coefficient with whole time segment at different structural natural frequencies. It can be seen two distinct frequencies, the main structural natural frequency and the secondary buffet frequency, as well as other higher harmonic frequencies. The system is highly nonlinear.

Different from the responses of lock-in in Fig. 10, the system responses do not behave a harmonic vibration any more to reach limit cycle oscillation, but exhibit divergent instability. And, the moment coefficient responses exhibit the fluid and structural mode interaction and competition with each other, as the whole process of moment coefficient at $k_\alpha = 0.39$ distinctly displays.

Following lock-in, when the structural natural frequency increases up to a sufficiently large value, far higher than the double buffet frequency, the pitch angle and moment coefficient curves spread back to a harmonic vibration, as shown in Fig. 12. The system goes into LCO again. The pitch angle amplitude is so small, reducing by about 1–2 level, that it has no impact on flow pattern. The moment coefficient amplitude is not large either, approximately equal to that of the rigid airfoil. The corresponding frequency content of moment coefficient is very simplex, just has one peak, which is fixed at the buffet frequency. It hints that the system coupling frequency is finally away from the structural natural frequency and returns to the buffet frequency again. The lock-in phenomenon vanishes.

4.2. Effect of the mass ratio on lock-in characteristic

To investigate the effect of mass ratio on lock-in characteristic of the elastic system, simulation is repeated for another different mass ration $\mu = 1000$, by using the above same method and computational state. The structural natural frequency varies from 0 to 0.55.

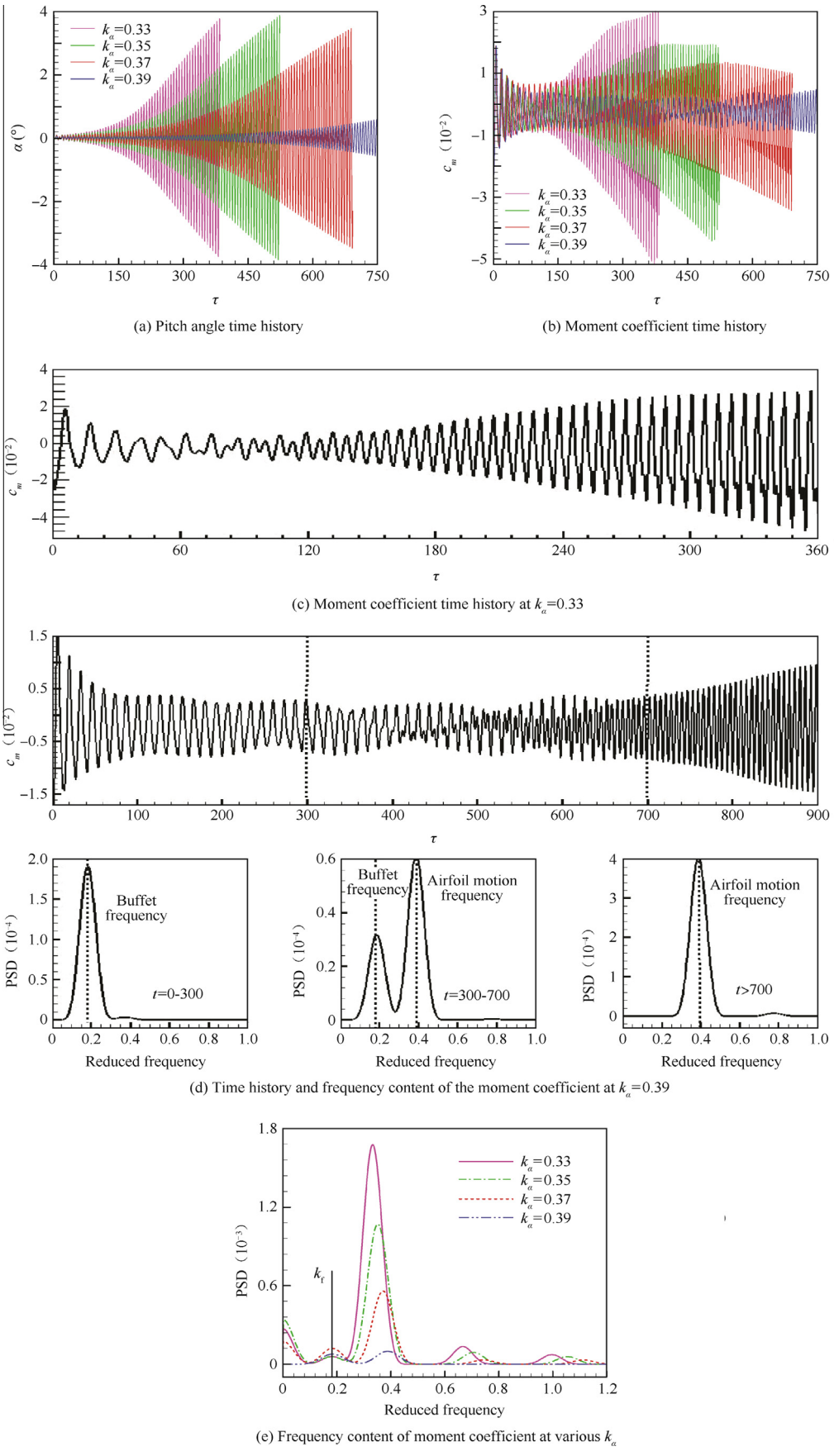

Fig. 11 Aeroelastic responses and frequency content of elastic system when structure frequency is near double buffet frequency.

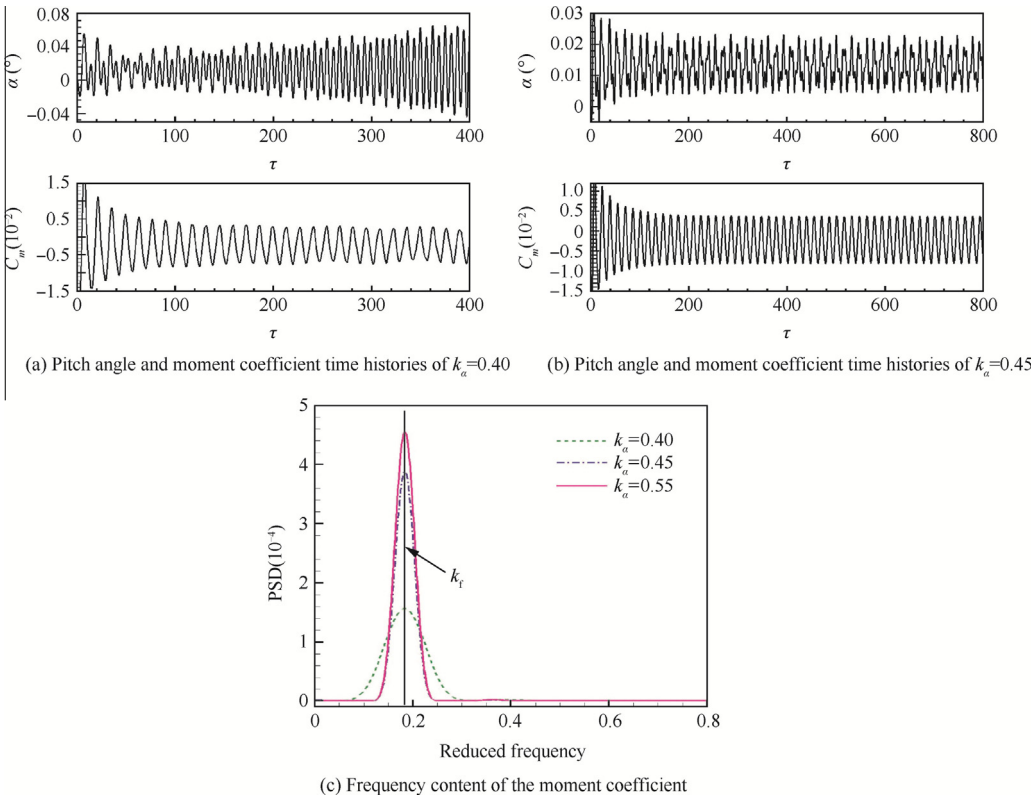

Fig. 12 Aeroelastic responses and frequency content of elastic system when structure frequency is far higher than double buffet frequency.

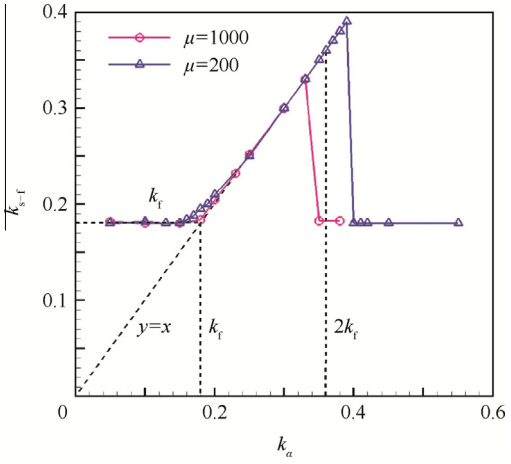

Fig. 13 Coupling frequency of elastic system at different structural natural frequencies with $\mu = 1000$ and $\mu = 200$.

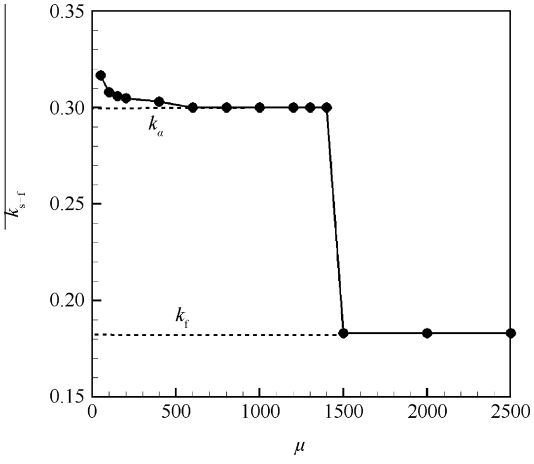

Fig. 14 Coupling frequency of elastic system at different mass ratios with $k_\alpha = 0.30$, $\zeta = 0$.

Fig. 13 shows the elastic system coupling frequency at various structural natural frequencies. It is shown that when the structural natural frequency is close to the buffet frequency, the system coupling frequency is equal to the structural natural frequency. The lock-in presents. The broad range of lock-in for the structural natural frequency is $0.18 < k_\alpha < 0.33$. When the structural natural frequency is beyond the range ($k_\alpha < 0.18$ or $k_\alpha > 0.33$), the lock-in disappears, and the system coupling frequency is back to the buffet frequency again.

By contrasting the results with those at $\mu = 200$, the aeroelastic response of the elastic system exhibits similar pattern and the lock-in appears and vanishes as the structural natural frequency changes. But differently, as mass ratio increases, the frequency range of lock-in gets narrow, with the upper threshold decreasing. However the lower threshold is always keeping the same.

To investigate the effect of mass ratio in detail, simulations are also conducted with zero structure damping, fixed

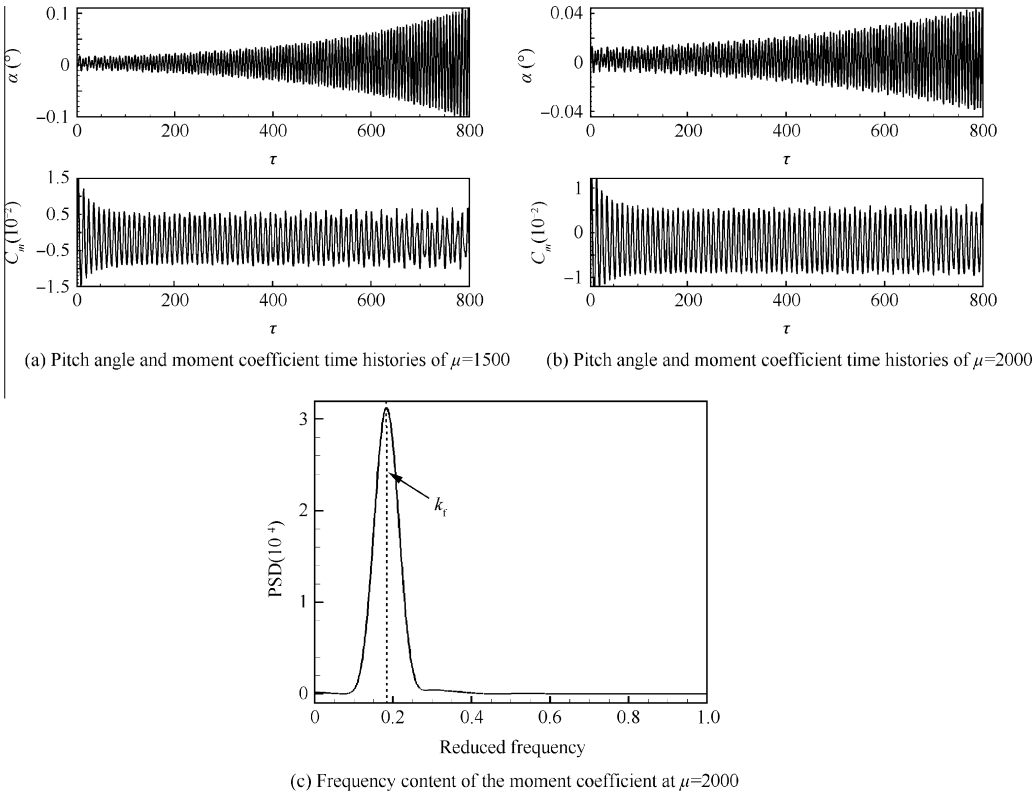

Fig. 15 Aeroelastic responses and frequency content of the elastic system at $\mu \geqslant 1500$.

structural natural frequency at $k_\alpha = 0.30$ and various mass ratios ranging from zero to two thousand. The computational conditions are $Ma = 0.7$, $\alpha_m = 4.8°$, $Re = 3.0 \times 10^6$, $r_\alpha^2 = 1.036$, $k_\alpha = 0.30$, $\zeta = 0$, $\mu = 0 - 2000$.

Fig. 14 shows the elastic system coupling frequency at different mass ratios. It is shown that as mass ratio changes, the elastic system exhibits different flow patterns. When mass ratio is lager than 1500, the system coupling frequency is equal to the buffet frequency, namely $k_{s-f} = k_f = 0.18$. While, when mass ratio is lower than 1500, the system coupling frequency locks into the structural natural frequency, namely $k_{s-f} = k_\alpha = 0.30$. The lock-in occurs. However, interestingly, when mass ratio is much lower than 400, the system coupling frequency is no longer equal to, but has a trend to leave away from the structural natural frequency and shifts towards the double buffet frequency, with mass ratio decreasing.

Figs. 15–17 show the aeroelastic responses of the coupling elastic system and the corresponding PSD analysis at different mass ratios in detail.

Mass ratio is the scale of the relative structural stiffness. When mass ratio is very large, the rigidity of the structure will become strong and the flexibility will get weak. The aerodynamic loads may cause very tiny structure elastic vibration, which is not sufficient to affect the flow property. As shown in Fig. 15, when $\mu \geqslant 1500$, the curve of pitch angle of attack is a little divergent with small displacement, not enough to influence the flow. The moment coefficient curve reveals harmonic vibration. Fig. 15(c) shows the frequency content of moment coefficient at $\mu = 2000$. There is only one peak at the buffet frequency. It means that the system coupling frequency is equal to the buffet frequency. The lock-in is not present.

As shown in Fig. 16, when $400 < \mu < 1500$ the pitch angle of attack curve is divergent, with a high divergence speed increasing with mass ratio falling, and the amplitude is larger than before. The responses of moment coefficient always experience a period of harmonic vibration at low frequency firstly, then spread slowly with high and low frequencies together, and finally get into divergent oscillation at high frequency. In this case, the system coupling frequency successfully locks into the structural natural frequency. The lock-in appears. The lower the mass ratio is, the quicker the structure elastic vibration spreads, and the shorter the moment coefficient will experience to reach lock-in.

Taking $\mu = 1000$ as an example, Fig. 16(c) presents the frequency analysis of the moment coefficient response at different time periods. In the first segment, the moment coefficient curve presents harmonic vibration and the buffet frequency dominates the response. In the second segment, the curve spreads slowly, and there are two peak frequency components, less power in the buffet frequency and more power in the structural natural frequency. The coupling frequency of the elastic system shifts towards the structural natural frequency. Finally, in the last segment, the curve diverges, and the response is solely in the structural natural frequency. Fig. 16(d) presents the frequency content of the whole time segment. There are two distinct frequencies, the secondary lower buffet frequency and the main higher structural natural frequency. The system coupling frequency gets the same value as the structural natural frequency. The lock-in presents.

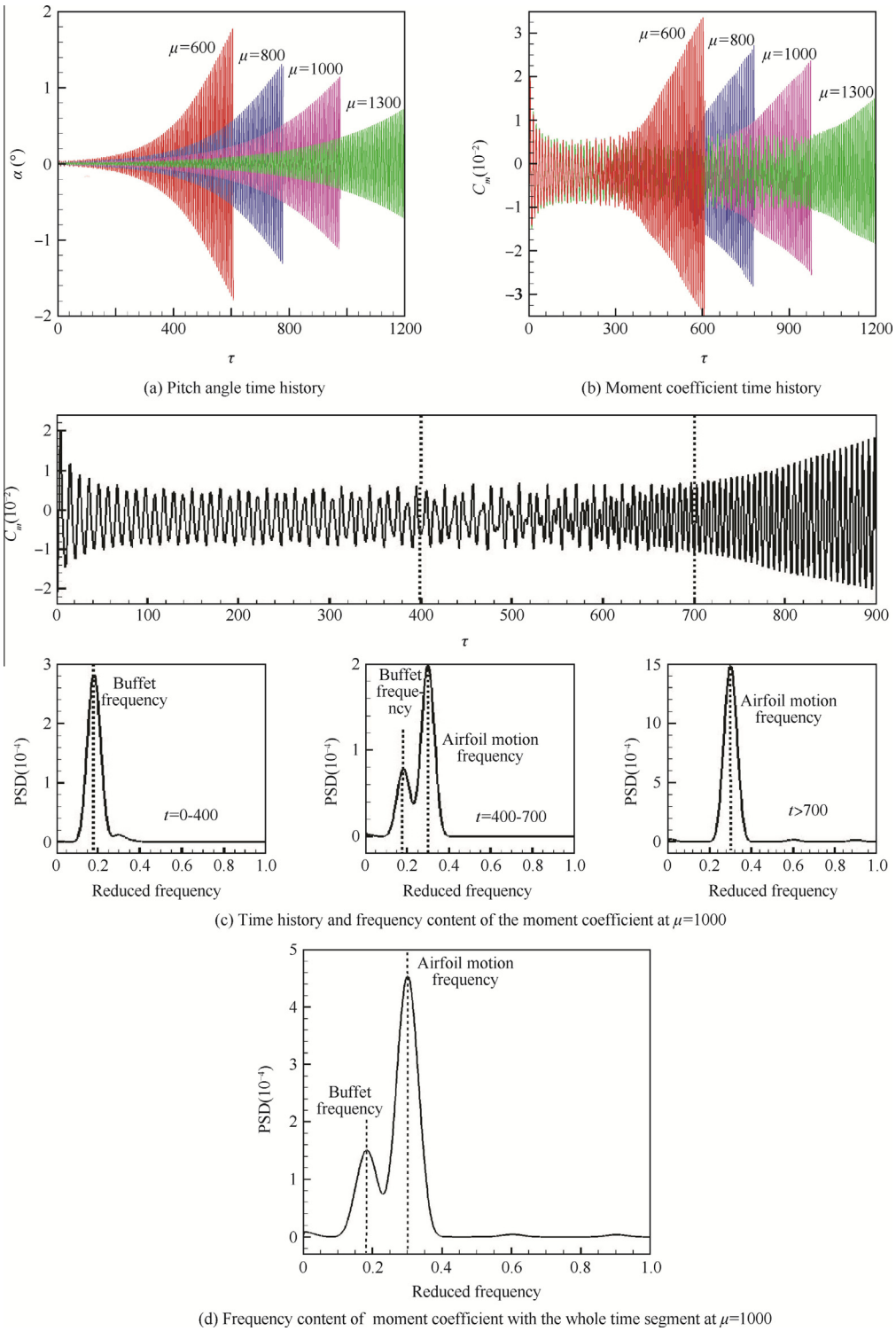

Fig. 16 Aeroelastic responses and frequency content of the elastic system at $400 < \mu < 1500$.

As mass ratio is much lower than 400, the elastic system comes into divergent instability rapidly. As shown in Fig. 17, the divergence speed and amplitude of the pitch angle and moment coefficient get greater, and the moment coefficient response does not behave harmonic vibration any more. Differently, the corresponding frequency content of moment coefficient is not equal to, but away from the structural natural frequency, and towards the double buffet frequency as mass ratio gets much smaller. Also, there are higher frequency components in the frequency content.

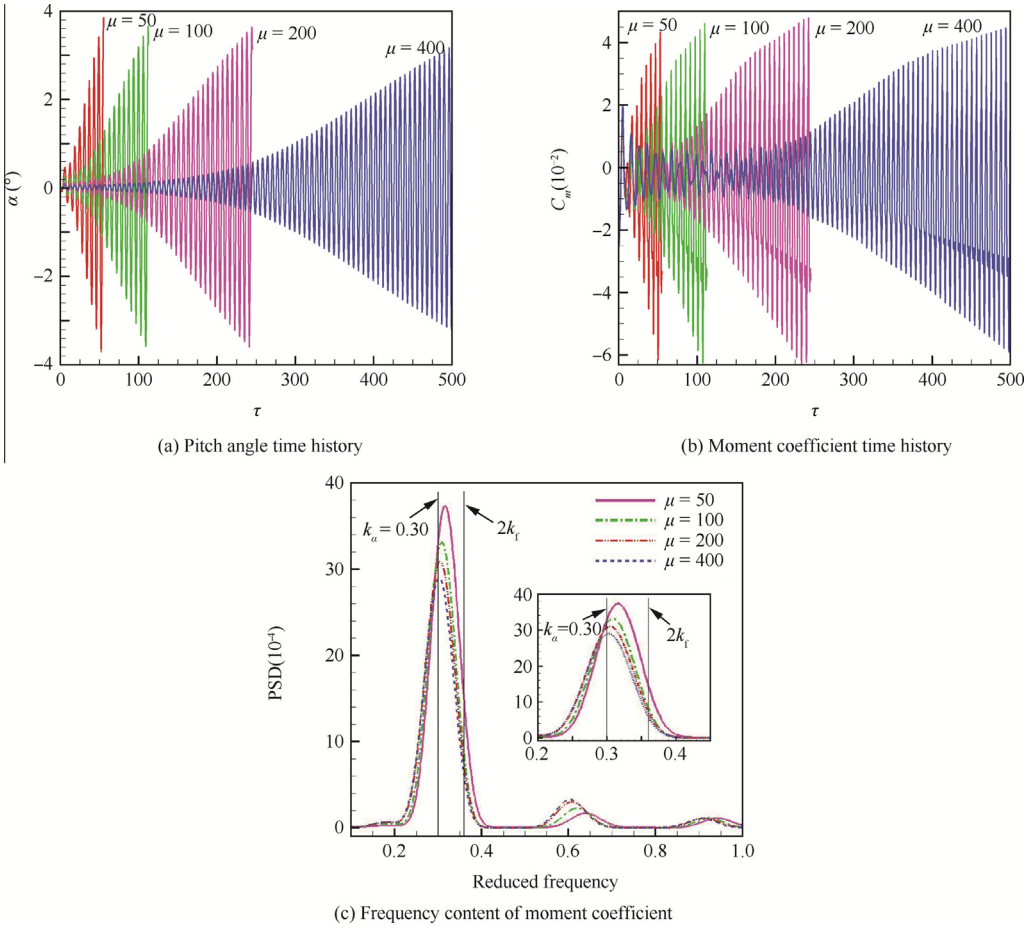

Fig. 17 Aeroelastic responses and frequency content of elastic system at $\mu < 400$.

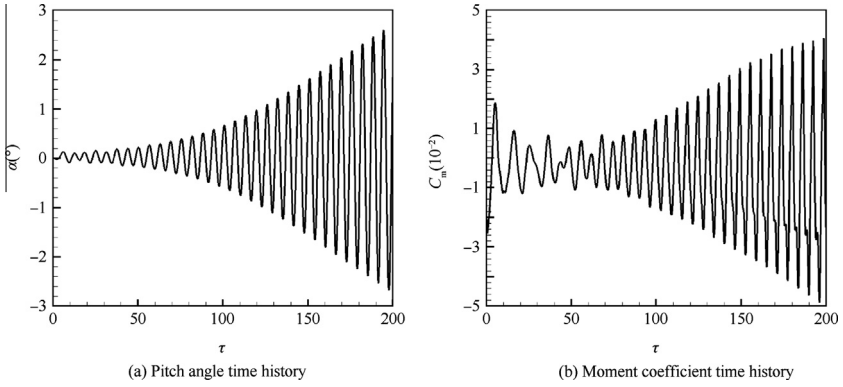

Fig. 18 Time histories of pitch angle and moment coefficient of elastic system at $k_\alpha = 0.30$, $\mu = 200$, no structural damping.

4.3. Effect of structural damping on lock-in characteristic

The structural damping has an effect on the stability of the elastic system, but it is ignored in the above computations. Figs. 18 and 19 show the aeroelastic responses of the elastic system with zero and added 1% structural damping respectively. The mass ratio and structural natural frequency are fixed. For the system with zero damping, the response is divergent. However, the responses with 1% damping diverge slowly and finally tend to be limit cycle oscillation. The structural damping delays the growth speed of the responses and reduces the amplitudes.

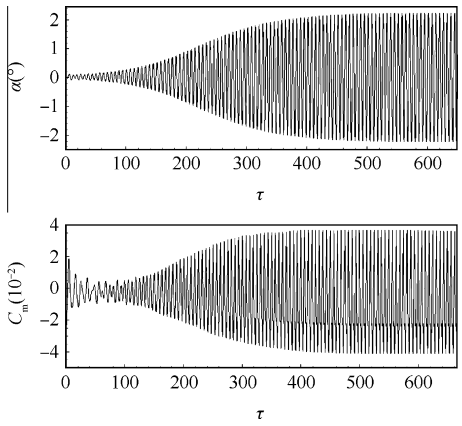

Fig. 19 Time histories of pitch angle and moment coefficient of elastic system at $k_\alpha = 0.30$, $\mu = 200$, 1% structural damping.

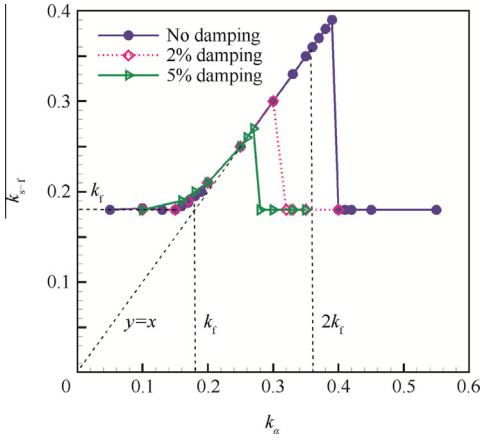

Fig. 20 Frequency range of lock-in of elastic system at various structural damping with $\mu = 200$.

Fig. 20 presents the frequency range of lock-in of the elastic system at various structural damping. The mass ratio is fixed at $\mu = 200$. As the structural damping increases, the range of lock-in gets narrow. The beginning point of the lock-in present almost keeps the same value, while the ending point decreases with the damping increasing.

5. Conclusions

In the current work, the lock-in characteristic in transonic buffet flow of an elastic airfoil is mainly concerned. Numerical simulations are performed to study the range of lock-in and the effects of the structural natural frequency, mass ratio and structural damping on lock-in characteristic.

(1) As the structural natural frequency changes, the aeroealstic responses of the elastic system in transonic buffet flow experience the lock-in phenomenon. The lock-in occurs as the structural nature frequency is close to the buffet frequency, and stays present until the structural nature frequency is near the double buffet frequency, and then vanishes when the structural nature frequency is far away the double buffet frequency. It hints that the lock-in presents in a wide range from near the buffet frequency to the double buffet frequency, with the elastic system coupling frequency equal to the structural natural frequency.

(2) The mass ratio and structural damping have a great impact on the frequency range of lock-in. The lower the mass ratio and structural damping are, the wider the range of lock-in will be. As the mass ratio and structural damping decrease, the upper threshold of lock-in gets greater, but the lower threshold almost never changes, which is always near the buffet frequency.

Further work will be carried out to study the lock-in mechanism by analyzing the eigenvalue of the system with unstable dynamic model.

Acknowledgement

This study was supported by the project of the Aerospace Innovation Foundation of China (No. 2014200013).

References

1. Lee BHK. Self-sustained shock oscillations on airfoils at transonic speeds. *Prog Aerosp Sci* 2001;**37**(2):147–96.
2. Crouch JD, Garbaruk A, Magidov D, et al. Origin of transonic buffet on aerofoils. *J Fluid Mech* 2009;**628**:357–69.
3. Crouch JD, Garbaruk A, Magidov D. Predicting the onset of flow unsteadiness based on global instability. *J Comput Phys* 2007;**224**(2):924–40.
4. Hartmann A, Feldhusen A, Schröder W. On the interaction of shock waves and sound waves in transonic buffet flow. *Phys Fluids* 2013;**25**(2):384.
5. Jacquin L, Molton P, Deck S, Maury B, Soulevant D. Experimental study of shock oscillation over a transonic supercritical profile. *AIAA J* 2009;**47**(9):1985–94.
6. Chen LW, Xu CY, Lu XY. Numerical investigation of the compressible flow past an aerofoil. *J Fluid Mech* 2010;**643**(3):97–126.
7. Xiao Q, Tsai HM, Liu F. Numerical study of transonic buffet on a supercritical airfoil. *AIAA J* 2006;**44**(3):620–8.
8. Iovnovich M, Raveh DE. Reynolds-averaged navier–stokes study of the shock-buffet instability mechanism. *AIAA J* 2012;**50**(4):880–90.
9. Barakos G, Drikakis D. Numerical simulation of transonic buffet flow using various turbulence closures. *Int J Heat Fluid Flow* 2000;**21**(5):620–6.
10. Deck S. Numerical simulation of transonic buffet over a supercritical airfoil. *AIAA J* 2005;**43**(7):1556–66.
11. Thiery M, Coustols E. Numerical prediction of shock induced oscillations over a 2D airfoil: Influence of turbulence modeling and test section walls. *Int J Heat Fluid Flow* 2006;**27**(4):661–70.
12. Steimle PC, Karhoff DC, Schröder W. Unsteady transonic flow over a transport-type swept wing. *AIAA J* 2012;**50**(2):399–415.
13. Raveh DE, Dowell EH. Frequency lock-in phenomenon for oscillating airfoils in buffeting flows. *J Fluids Struct* 2011;**27**(1):89–104.
14. Raveh DE. Numerical study of an oscillating airfoil in transonic buffeting flows. *AIAA J* 2009;**47**(3):505–15.
15. Iovnovich M, Raveh DE. Transonic unsteady aerodynamics in the vicinity of shock-buffet instability. *J Fluids Struct* 2012;**29**(1):131–42.
16. Nitzsche J, Giepman RHM. Numerical experiments on aerodynamic resonance in transonic airfoil flow. In: Dillmann A, editor. *New results in numerical and experimental fluid mechanics*. Berlin: Springer-Verlag; 2013. p. 349–57.

17. Young J, Lai JCS. Vortex lock-in phenomenon in the wake of a plunging airfoil. *AIAA J* 2007;**45**(2):485–90.
18. Hartmann A, Klaas M, Schröder W. Coupled airfoil heave/pitch oscillations at buffet flow. *AIAA J* 2013;**51**(7):1542–52.
19. Raveh DE, Dowell EH. Aeroelastic responses of elastically suspended airfoil systems in transonic buffeting flows. *AIAA J* 2014;**52**(5):926–34.
20. Blom F, Leyland P. Analysis of fluid-structure interaction on moving airfoils by means of an improved ALE-method. Reston: AIAA; 1997. Report No.: AIAA-1997-1770.
21. Wang G, Jiang YW, Ye ZY. An improved LU-SGS implicit scheme for high reynolds number flow computations on hybrid unstructured mesh. *Chin J Aeronaut* 2012;**25**(1):33–41.
22. de Boer A, van der Schoot MS, Bijl H. Mesh deformation based on radial basis function interpolation. *Comput Struct* 2007;**85**(11–14):784–95.
23. Zhang WW, Jiang YW, Ye ZY. Two better loosely coupled solution algorithms of CFD based aeroelastic simulation. *Eng Appl Comput Fluid Mech* 2007;**1**(4):253–62.
24. Williamson CHK, Govardhan R. Vortex-induced vibrations. *Annu Rev Fluid Mech* 2004;**36**(444):413–55.
25. Anagnostopoulos P, Bearman PW. Response characteristics of a vortex-excited cylinder at low reynolds numbers. *J Fluids Struct* 1992;**6**(1):39–50.
26. Carlson HA, Feng JQ, Thomas JP, et al. Computational models for nonlinear aeroelasticity. *Proceedings of the 43rd AIAA aerospace sciences meeting and exhibit*; 2005 Jan 10-13; Reno, Nevada. Reston: AIAA; 2005.
27. Singh SP, Mittali S. Vortex-induced oscillations at low reynolds numbers: hysteresis and vortex-shedding modes. *J Fluids Struct* 2005;**20**(8):1085–104.
28. Barbut G, Braza M, Miller M, et al. NACA0012 with aileron. In: Doerffer P, Hirsch C, Dussauge JP, Babinsky H, editors. *Unsteady effects of shock wave induced separation*. Berlin: Springer-Verlag; 2010. p. 101–31.

Quan Jingge is a Ph.D. candidate at School of Aeronautics, Northwestern Ploytechnical University. She received her B.S. and M.S. degrees from Northwestern Ploytechnical University in 2008 and 2011 respectively. Her main research interests are aeroelastic analysis and computational fluid dynamics.

Zhang Weiwei is a professor and Ph.D. supervisor in Northwestern Ploytechnical University. His current research interests are aeroelasticity and computational fluid dynamics.

Gao Chuanqiang is a Ph.D. candidate at School of Aeronautics, Northwestern Ploytechnical University. His area of research includes aeroelastic study.

Ye Zhengyin is a professor and Ph.D. supervisor at School of Aeronautics, Northwestern Ploytechnical University. His current research interests are computational fluid dynamics, aerodynamics and aeroelasticity.